Available online at www.sciencedirect.com
SCIENCE DIRECT®
Thermochimica Acta 412 (2004) 13–23
thermochimica acta
www.elsevier.com/locate/tca

Thin-film differential scanning nanocalorimetry: heat capacity analysis

M.Yu. Efremov, E.A. Olson, M. Zhang, S.L. Lai, F. Schiettekatte, Z.S. Zhang, L.H. Allen*

Department of Materials Science and Engineering and the Coordinated Science Laboratory at the University of Illinois at Urbana-Champaign, 1101 W. Springfield Avenue, Urbana, IL 61801, USA

Received 6 June 2003; received in revised form 21 August 2003; accepted 27 August 2003

Abstract

This paper analyses the electrical response of a quasi-adiabatic, thin-film nanocalorimeter system for the purpose of obtaining values of the heat capacity of ultra-thin samples. The pulse-heating method of heat capacity measurement is based on the observation of the temperature rise during the heating of the sample by a pulse of current. By measuring the voltage and current (in differential mode) of both reference and sample cells of the calorimeter during the pulse, the heat capacity is obtained. Also described are different methods to derive corrections for the baseline to account for the non-ideal differences between the reference and sample cells characteristics, including differences in addendum and resistance–temperature response. Further analysis accounts for the actual heat loss during the measurement, shunting effects of current through the substrate, and heat capacity of the blank calorimeter. Examples of the effects of each of the non-ideal conditions are given.

Keywords: Nanocalorimetry; Thin films; Heat capacity analysis

1. Introduction

The pulse-heating method of heat capacity measurement is based on the observation of the temperature rise during the heating of the sample by a pulse of current. The electric power of the current is known and experimental conditions should be close to adiabatic. This method has been used for many years [1]. One of the important advantages of the technique is its simplicity. The calorimeter often consists only of the sample itself (in the form of wire or strip). This type of calorimeter makes it possible to measure the thermal properties of a sample over a wide range of temperatures and to characterize small amounts of substance. Applications of the method include: measurements of thermal properties at temperatures up to 3600 °C [1–3] and heating rates up to 10^7 K/s [4], kinetics of decomposition at high heating rates [5], and critical temperature and pressure measurements [6].

Development of the membrane-based calorimeter ([7], for example; see also [8]) has been a significant advance in the field. Fabrication of a calorimetric sensor on a thin membrane grown on a Si wafer using standard microlithography methods produces a sensor with an extremely small addenda. Using this approach, we developed a novel calorimetric technique—thin-film DSC nanocalorimetry (TDSC) ([9] and references therein), which allows us to measure thermal effects in various nanometer-thick films.

The scope of this article is the heat capacity analysis used in the nanocalorimetry technique. While the physics of TDSC method are simple, non-trivial methods of data processing are required in order to get dependable results. The basic theory of heat capacity calculations in the TDSC method is straightforward [10,11], but it gives typically semi-quantitative values. Random noise, introduced mostly by differentiation of digitized data, is the typical problem and can be addressed by improved numerical procedure. Other factors able to deteriorate the quality of results, and can be sufficiently compensated by proper calculation procedures, are—a mismatch between sample and reference sensor; the need for baseline correction for massive samples, heat loss issues, and errors caused by non-ideality of calibration procedure. While unavoidable, these deviations can be substantially reduced by using specific models.

In this paper we give detailed descriptions of these problems and how can they be reduced or eliminated by using specific calculation methods. Some uncertainties of the TDSC method strongly depend on the experimental hardware; these topics are discussed elsewhere [12]. The

* Corresponding author. Tel.: +1-217-333-7918; fax: +1-217-244-163,
E-mail address: L-ALLEN9@uiuc.edu (L.H. Allen).

0040-6031/$ – see front matter © 2003 Elsevier B.V. All rights reserved.
doi:10.1016/j.tca.2003.08.019

fabrication and design considerations of the TDSC sensor are described elsewhere [8].

2. TDSC: principles of operation

The TDSC sensor, schematically shown in Fig. 1, is a silicon-based chip made by standard microfabrication technology. It consists of a thin, free-standing membrane of SiN_x supported by a Si frame. Typical dimensions of the membrane are 30–50 nm in thickness and several millimeters in lateral dimensions. A thin, typically 50 nm thick, metal (usually Pt, Au, Al or Ni) strip is deposited onto one side of the membrane. A sample is deposited either on the metal strip directly (if it is not conductive and does not react with the metal) or on the opposite, membrane covered side. During the DSC scan, a pulse of current through the metal strip causes a temperature rise due to Joule heating. Using metal with a significant temperature coefficient of resistance (TCR), the metal strip is operated also as a resistance temperature detector (RTD). The working part of the strip and the membrane beneath it form a calorimetric cell. The small thicknesses of the constituents and the combination of the heater and thermometer functions in one component provide an exceptionally low addenda of the cell, which is the key reason for the high sensitivity of TDSC. The cell works in a nearly adiabatic mode, which assumes high heating rates with typical values of tens of K/ms.

Two sensors, sample and reference, are used in the differential scheme, illustrated in Fig. 2. The DSC scan is initiated by passing simultaneous current pulses through the heaters. Fig. 3 shows typical, raw, experimental data. Currents through the heaters $I_S(t)$ and $I_R(t)$ (Fig. 3(1)), voltages $V_S(t)$ and $V_R(t)$ (Fig. 3(2)) across them, and differential voltage $\Delta V(t)$ (Fig. 3(5)) are sampled by high frequency analog-to-digital converters. The indices S and R denote sample and reference, respectively, and t is time. The resistances of sensors' heaters $R_S(t)$ and $R_R(t)$ (Fig. 3(3)) are calculated using current and voltage data. Then the temperatures of calorimetric cells $T_S(t)$ and $T_R(t)$ (Fig. 3(4)) are calculated using resistances $R_S(t)$ and $R_R(t)$ and calibration functions $T_S(R_S)$ and $T_R(R_R)$. Prior to the experiment, the heater resistances of both sensors R_S and R_R are calibrated against temperature T in a vacuum three-zone tube furnace and analytical forms of the functions $T_S(R_S)$ and $T_R(R_R)$ are determined. The derivative of ΔV over time (Fig. 3(5)) contains most of the information about thermal processes in the sample and is useful for real-time control of the DSC scan. Finally, the heat capacity of the sample C_P^{SMP} as a function of temperature (calorimetric curve) is calculated (Fig. 3(6)).

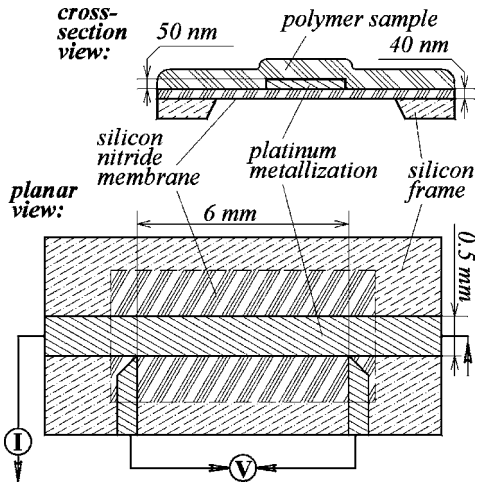

Fig. 1. Cross-section and planar views of a typical TDSC sensor with a polymer sample on it (not to scale).

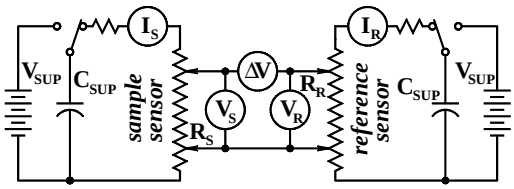

Fig. 2. Principal electric diagram for TDSC measurement.

3. Analysis of heat capacity

3.1. Calculation of heat capacity using raw current and voltage data: method I (main)

Under adiabatic conditions, all Joule heat will be consumed to increase the temperature of the calorimetric cell:

$$V(t)I(t)\,\mathrm{d}t = C_P(T)\,\mathrm{d}T \tag{1}$$

Introducing heating rate $v(t) = \mathrm{d}T/\mathrm{d}t$, for reference and sample cells, we find

$$C_P^{\mathrm{AD,R}}(T_R(t)) = \frac{V_R(t)I_R(t)}{v_R(t)} \tag{2a}$$

and

$$C_P^{\mathrm{AD,S}}(T_S(t)) + C_P^{\mathrm{SMP}}(T_S(t)) = \frac{V_S(t)I_S(t)}{v_S(t)}, \tag{2b}$$

where $C_P^{\mathrm{AD,R}}$ and $C_P^{\mathrm{AD,S}}$ are the heat capacities of the reference and sample cells. Subtracting Eq. (2a) from Eq. (2b), one gets

$$C_P^X(T_S(t)) \equiv C_P^{\mathrm{SMP}}(T_S(t)) + [C_P^{\mathrm{AD,S}}(T_S(t)) - C_P^{\mathrm{AD,R}}(T_R(t))] \tag{3a}$$

$$C_P^X(T_S(t)) = \frac{V_S(t)I_S(t)}{v_S(t)} - \frac{V_R(t)I_R(t)}{v_R(t)} \tag{3b}$$

Generally, values C_P^X and C_P^{SMP} are nearly, but not quite, equal. C_P^X can be calculated using data from a given calorimetric scan, but the C_P^{SMP} is the heat capacity of sample that we are interested in. These values are identical under two important assumptions.

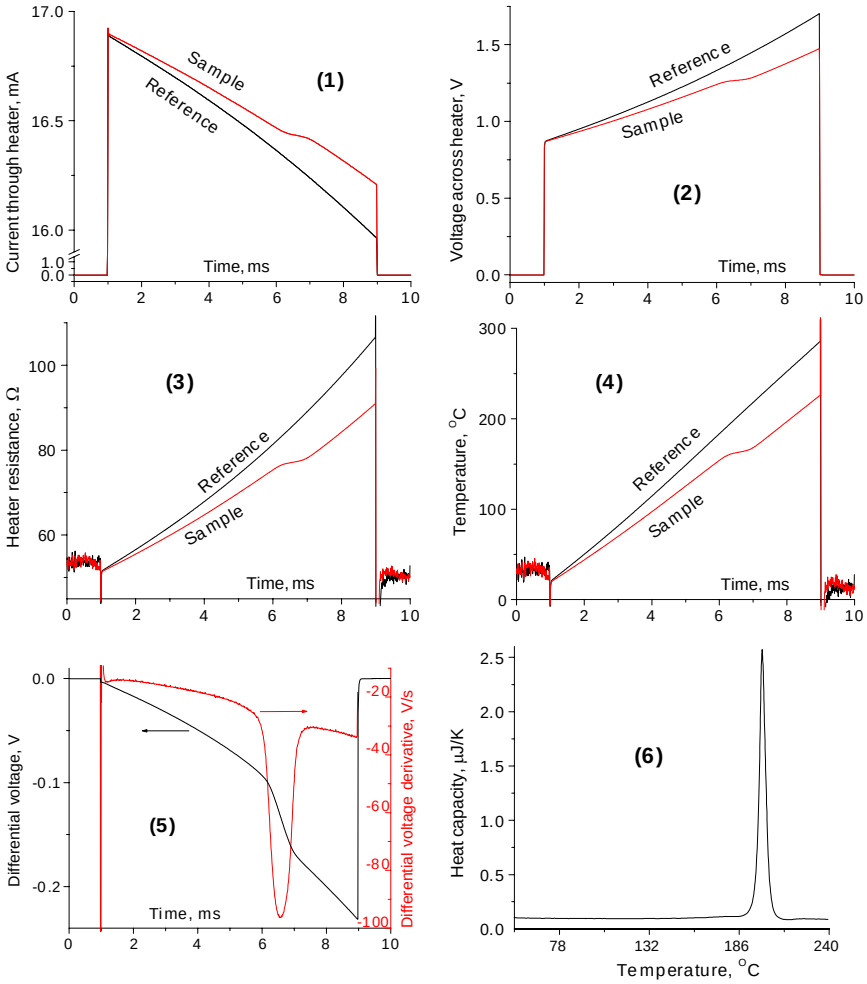

Fig. 3. Raw experimental data (1–5) and final result (6) for TDSC measurement of a 20 nm In film deposited on the sensor with Ni metallization. The current pulse of 8 ms duration starts at the time 1 ms. Current through heaters (1), voltage across them (2), heater resistances (3) and temperatures (4) for both sample and reference sensors are shown. Data for resistance and temperature are not valid when the current is absent (<1 ms and >9 ms). (5) demonstrates differential voltage and its derivative over time, and (6) shows the calorimetric curve of the sample, calculated using the main method with corrections 1–3.

1. Both the sample and reference sensors have the same addenda:

$$C_P^{\mathrm{AD,S}}(T) = C_P^{\mathrm{AD,R}}(T) \equiv C_P^{\mathrm{AD}}(T). \quad (4)$$

2. The difference between T_R and T_S at each t is small, and the $C_P^{\mathrm{AD}}(T)$ function is flat enough to assume that:

$$C_P^{\mathrm{AD}}(T_\mathrm{R}) = C_P^{\mathrm{AD}}(T_\mathrm{S}). \quad (5)$$

The errors caused by these assumptions can be eliminated, as described in Section 3.3. Here we consider the ways to evaluate C_P^X.

A differential mode of measurement is not necessary to use Eq. (3b) for C_P^X calculation. However, rewriting Eq. (3b) as

$$C_P^X(T_\mathrm{S}(t)) = \frac{V_\mathrm{R}(t) I_\mathrm{R}(t)}{v_\mathrm{R}(t)} \times \left[\left(\frac{V_\mathrm{S}(t) I_\mathrm{S}(t)}{V_\mathrm{R}(t) I_\mathrm{R}(t)} \times \frac{1}{v_\mathrm{S}(t)/v_\mathrm{R}(t)} \right) - 1 \right], \quad (6)$$

we see that the expression for C_P^X contains the noisy component $v_\mathrm{S}/v_\mathrm{R} = \mathrm{d}T_\mathrm{S}/\mathrm{d}T_\mathrm{R}$. This statement requires additional comment. Differentiation is a "notoriously unsatisfactory process" [13], which exaggerates irregularities in a function being differentiated. This is true both for numerical operations [13,14] and analog processes [15,16]. Such irregularities can be developed by numerous reasons—thermal noise in conductors, transients in electrical contacts, quantization errors in analog-to-digital conversion, to name a few, and tend to be of relatively high frequency. The output of a differentiation is proportional to frequency. For example, for the harmonic signal $A \sin wt$ the output is $Aw \cos wt$, where A is the amplitude and w is the angular frequency of the signal. Comparing a Nyquist frequency of 50 kHz (typical for our experiments) and a typical time scale for thermal processes in the calorimetric cell of a millisecond (of the order of 1 kHz of corresponding frequency), it is clear that the differentiation process can degrade the signal-to-noise ratio by 1–2 orders of magnitude. Practically, derivatives are

the major sources of noise in the calorimetric curves. Therefore, below, we will concentrate on the errors introduced by derivatives. It should be mentioned here, that Eq. (6) has, except dT_S/dT_R, also $v_R = dT_R/dt$ derivative, which is also significant source of noise. Nevertheless, the attenuation of noise in the v_R component is much simpler, because (a) the dt interval in sampling process is fixed and well stabilized, and (b) since the reference sensor has no sample on it, the v_R is a featureless and monotonic function of temperature, which can be smoothed by accumulation of many measurements and by approximation. These issues will be discussed later.

To improve noise characteristics introduced by v_S/v_R term in Eq. (6), let us express this component using differential voltage $\Delta V(t)$. Differentiating the expression $\Delta V = V_S - V_R$, one can find that

$$\frac{d\Delta V}{dt} = v_S(t) \left.\frac{dV_S}{dT}\right|_t - v_R(t) \left.\frac{dV_R}{dT}\right|_t, \tag{7}$$

or, expressing v_S/v_R explicitly

$$\frac{v_S(t)}{v_R(t)} = \frac{d\Delta V/dt}{v_R(t)(dV_S/dT)|_t} + \frac{(dV_R/dT)|_t}{(dV_S/dT)|_t}. \tag{8}$$

While the derivative of ΔV contains the major component of the useful signal, the derivatives of V_S and V_R are major sources of noise. Using $V = IR$, one can find

$$\left.\frac{dV}{dT}\right|_t = I(t) \left.\frac{dR}{dT}\right|_t + R(t) \left.\frac{dI}{dT}\right|_t, \tag{9}$$

which is valid for both the reference and sample terms. The $R(T)$ function, obtained from the calibration procedure, has an analytical form. Consequently, the noise, introduced by the first term in the right side of Eq. (9), is negligible. The most noisy component in Eq. (9), the derivative of current, is small and depends on hardware design. In the ideal case of a stable current source with an infinite impedance, the current through the heater would be constant, and the last term of Eq. (9) would be zero. In the real situation, the current can be approximated well by using an empirical function. The form of this function could be chosen using electric diagram considerations.

For the scheme shown in Fig. 2, a good approximation is given by

$$I_{APP}(t) = \frac{V_{SUP} - (Q(t)/C_{SUP})}{R_{CONST} + R(t)(1 + a + bR(t))}, \tag{10}$$

where V_{SUP} is the voltage on the charged capacitor before the pulse, C_{SUP} the effective electric capacity of the capacitor, R_{CONST} the resistance in heater chain which is not dependent on temperature, a and b are constants, and $Q(t)$ is the discharge of the capacitor during the pulse

$$Q(t) = \int_0^t I(\tau)d\tau, \tag{11}$$

calculated from the experimental $I(t)$ data.

In this case, the derivative of current in Eq. (9), can be approximated by

$$\left.\frac{dI_{APP}}{dT}\right|_t = \frac{I^2(t)}{V_{SUP} - (Q(t)/C_{SUP})} \times \left[\frac{1}{v(t)C_{SUP}} + \left.\frac{dR}{dT}\right|_t (1 + a + 2R(t)b)\right]. \tag{12}$$

In practice, C_{SUP} is less than the nominal value of the capacitor. It should be determined experimentally for given hardware by nonlinear fitting of $I(t)$ by Eq. (10). Parameters a and b are calculated for each measurement by the least square fitting of current derivative using Eq. (12). Then, using the same equation with calculated a and b, the smooth approximation of dI/dT for Eq. (9) can be found.

Finally, Eq. (6) can be slightly improved using ΔV instead of V_R:

$$C_P^X(T_S(t)) = \frac{V_R(t)I_R(t)}{v_R(t)} \times \left[\frac{1}{v_S(t)/v_R(t)} \times \left(\frac{\Delta V(t)}{V_R(t)} + 1\right) \times \frac{I_S(t)}{I_R(t)} - 1\right]. \tag{13}$$

To summarize this section, the main method for calculating the sample heat capacity from electrical measurements in a DSC scan includes Eqs. (8), (9) and (13), and the approximation given by Eq. (12). All intermediate calculations should be performed in the time domain, which is expressed explicitly in the equations of this section. Conversion of heat capacity to the temperature domain is the last step of calculations.

Special care should be taken in proper handling of noisy data. After some mathematical manipulations on data with occasionally small signal-to-noise ratio, the initially random noise can be transformed to non-random one and consequent smoothing of such data would give wrong results. In the described method, the most sensitive parameter is the sample heating rate v_S and correlated variables (v_S/v_R). At sharp endothermic events (melting of crystals, for example), the sample temperature would be almost constant over the time of the transition. In this case, v_S would be close to zero and even small noise will cause the reciprocal value $1/v_S$ to achieve unlimitedly high values, including negative ones. Averaging such data would give wrong results.

The form of Eqs. (8) and (13) allows us to avoid v_S in the denominators of these expressions. The v_S in the sample case of Eq. (12) should be properly smoothed. The derivatives in Eq. (8) should also be smoothed. In our calculations, we use the simplest symmetrical box averaging in time domain

$$\bar{x}(t_i) = 1/t_{BOX} \int_{\tau=(t_i - t_{BOX})/2}^{\tau=(t_i + t_{BOX})/2} x(\tau)d\tau$$

and in temperature domain

$$\bar{x}(t_i) = \frac{1}{T_{BOX}} \int_{T=(T(t_i) - T_{BOX})/2}^{T=(T(t_i) + T_{BOX})/2} x(T)dT.$$

Since the data are measured at a fixed sampling rate (with fixed time interval Δt between measurements), the averaging in the time domain is equivalent to averaging of corresponding number of data points. According to our tests, using a mixture of time and temperature domain averaging is more effective than averaging all variables in only a single domain. A typical box size for averaging v (in Eqs. (8) and (12)) and dI/dT (approximated by Eq. (12)) is $T_{BOX} = 5$ K. For averaging of dV_S/dT (in Eq. (8)), I_S/I_R (in Eq. (13)), and final C_P values $t_{BOX} = 10$–90 μs (or 1–9 data points in case of a 100 kHz sampling rate), depending on heating rate. Additional averaging of the last term in Eq. (8) has $t_{BOX} = 50$–600 μs (5–60 data points).

Note that box averaging of derivatives is not effective enough:

$$\left.\overline{\frac{\mathrm{d}X}{\mathrm{d}t}}\right|_k \approx \frac{1}{2a+1}\sum_{i=k-a}^{i=k+a}\frac{X_{i+1}-X_i}{\Delta t} = \frac{X_{k+a+1}-X_{k-a}}{(2a+1)\Delta t}$$

(where $2a + 1$ is the box size), because information only from the first and the last points of the averaging interval is used. As a simple solution, in the case of derivatives we perform the averaging twice, although more accurate (and complicated) procedures could be employed.

Transient processes cause erroneous data points at the beginning and the end of DSC scan. Such data should be carefully removed prior to calculations: even one strongly outlying data point can disturb the whole $C_P(T)$ plot, due to the fitting procedure used for the evaluation of a and b in Eq. (12).

3.2. Calculation of heat capacity using raw current and voltage data: simplified methods

The main method described above, although accurate, requires an appreciable amount of calculation and the availability of all five sets of experimental data—$I_S(t)$, $I_R(t)$, $V_S(t)$, $V_R(t)$, and $\Delta V(t)$. Simplification of the method I can be useful.

3.2.1. Method II

In the case of an ideal current source, the current through the heater during a scan would be constant. In the case of two identical sources for both sample and reference sensors, we can assume $I_S = I_R$, or equivalently, $R_S(t) = R_R(t)[V_S(t)/V_R(t)]$. Using the definition $\Delta V = V_S - V_R$, we can express R_S as a function of R_R, V_R, and ΔV

$$R_S(t) = R_R(t)\left(1 + \frac{\Delta V(t)}{V_R(t)}\right). \tag{14}$$

and calculate the noisy term

$$\frac{v_S(t)}{v_R(t)} = \left.\frac{\mathrm{d}T_S(R_S(t))}{\mathrm{d}T_R(R_R(t))}\right|_t \tag{15}$$

using $R_S(t)$ from Eq. (14). Doing so, we replace two non-correlated noise sources (experimental R_S and R_R) by mutually correlated ones (R_S, calculated by Eq. (14) and experimental R_R). As a result, the noise is reduced.

Additionally, using the supposition $I_S = I_R$, Eq. (13) can be simplified

$$C_P^X(T_S(t)) = \frac{V_R(t)I_R(t)}{v_R(t)} \times \left[\frac{1}{v_S(t)/v_R(t)} \times \left(\frac{\Delta V(t)}{V_R(t)} + 1\right) - 1\right]. \tag{16}$$

Only 3 sets of data—$I_R(t)$, $V_R(t)$, and $\Delta V(t)$—are needed for this method. The additional assumption that $T(R)$ dependencies for both sensors are identical would simplify the experiment even more. Unlike sample sensors, which should be typically discarded after experiment, the reference sensor can be reused. Temperature calibration, performed once for a sensor, does not need to be repeated for any experiments where this sensor will be used as a reference.

3.2.2. Method III

Assuming that $I_S = I_R$ = constant and $T_S(R) = T_R(R)$, Eq. (8) can be rewritten as:

$$\frac{v_S(t)}{v_R(t)} = \frac{\mathrm{d}\,\Delta V/\mathrm{d}t}{v_R(t)I(\mathrm{d}R/\mathrm{d}T)|_t} + 1. \tag{17}$$

If the signal (d ΔV/dt) is small, Eq. (17) can be approximated as:

$$\frac{1}{v_S(t)/v_R(t)} \approx 1 - \frac{\mathrm{d}\,\Delta V/\mathrm{d}t}{v_R(t)I(\mathrm{d}R/\mathrm{d}T)|_t}, \tag{18}$$

Combining Eqs. (13) and (18), using $I_S = I_R$, and neglecting ΔV in Eq. (13), one can find

$$C_P^X(T(t)) = -\frac{V_R(t)}{v_R^2(t)\mathrm{d}R/\mathrm{d}T|_t}\frac{\mathrm{d}\,\Delta V}{\mathrm{d}t}. \tag{19}$$

This formula also requires only three sets of data—$I_R(t)$, $V_R(t)$, and $\Delta V(t)$. Moreover, Eq. (19) demonstrates that the sample heat capacity is proportional to d ΔV/dt. The coefficient in front of the d ΔV/dt term is nearly constant and can be approximated as a linear function of temperature:

$$C_P^X(T(t)) = (\alpha + \beta T)\frac{\mathrm{d}\,\Delta V}{\mathrm{d}t}. \tag{20}$$

Eq. (20) allows the combination of accuracy of the main method with the low noise character of the raw differential voltage signal. In this case, α and β are fitted using $C_P^X(T)$ determined by the main method. Then, a low-noise heat capacity can be calculated from Eq. (20), using these values of α and β. For strong signals this method gives only qualitative results.

3.2.3. Comparison of methods

Fig. 4 illustrates the difference between the main method I and the simplified methods II and III. A simple simulation program was used to calculate all five datasets measured during a calorimetric experiment, given $C_P(T)$ behavior for a sample and two typical sensors. Then, $C_P(T)$ was calculated

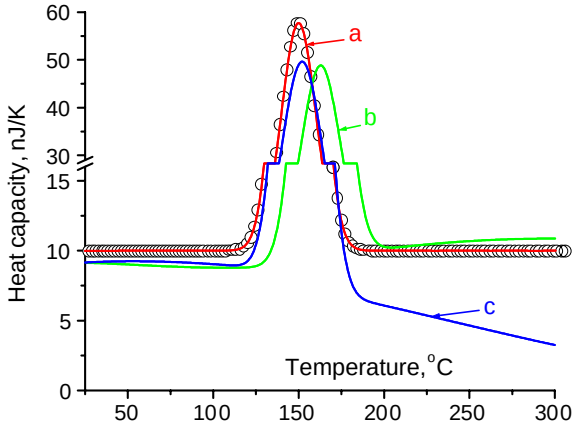

Fig. 4. Calorimetric curves calculated by different methods. Calculations use computer simulated raw data. (○)—imitated sample $C_P(T)$ dependence, close to the experimental curve for 2 nm In film. Methods used for backward calculation: (a) main method I, (b) simplified method II, (c) simplified method III. In the raw data generation, two sensors are simulated; these sensors have different $T(R)$ characteristics and equal addenda heat capacities, which do not depend on temperature. For all methods the 1st correction is made.

using these simulated datasets using the different methods. This procedure is also very useful for testing calculation software. For sensors with equal constant addenda $C_P^{\mathrm{AD,S}} = C_P^{\mathrm{AD,R}}$, only the first correction (see below) is needed for accurate calculation (the current version of our simulation program does not take heat loss into account). Fig. 4 demonstrates that the main method is the most accurate. Comparing methods II and III, usually it tends to be, that method II gives more accurate C_P values, while temperature of the features on the $C_P(T)$ plot is better represented by method III. Methods II and III are typically more accurate in calculating the integral heat of thermal processes than in calculating absolute heat capacity values. For the example shown in Fig. 4, the heat of fusion values given by methods II and III are 1.10 and 1.15 μJ (respectively), which are within the error of 10% of the accurate value of 1.20 μJ (while the heat capacity values are deviated much larger—more than 50% for the curve (c)).

3.3. Corrections using an idle experiment

Measurements on the calorimetric cells without any sample (an "idle experiment") can significantly improve the accuracy of the final $C_P(T)$. Corrections that can be made using data from such an idle experiment are discussed in this section.

3.3.1. Correction for different addenda

The error caused by the assumption in Eq. (4) can be corrected using an idle experiment made under the same conditions and with the same sensors as the subsequent measurements with the sample. Using the main method for idle experiment data, one can determine a baseline:

$$C_P^{X1}(T_{\mathrm{S0}}(t)) = C_P^{\mathrm{AD,S}}(T_{\mathrm{S0}}(t)) - C_P^{\mathrm{AD,R}}(T_{\mathrm{R}}(t)), \tag{21}$$

which reflects the difference between sensors in differential assembly. Note that the temperature dependence for the sample sensor in the idle experiment $T_{\mathrm{S0}}(t)$ is different that in the experiment with sample, while the $T_{\mathrm{R}}(t)$ functions are the same. Subtracting the $C_P{}^{X1}$ correction from the value obtained in the experiment with sample (see Eq. (3a)), one can get

$$\begin{aligned} C_P^{X\mathrm{Corr1}}(T_{\mathrm{S}}(t)) &= C_P^{X}(T_{\mathrm{S}}(t)) - C_P^{X1}(T_{\mathrm{S0}}(t)) \\ &= C_P^{\mathrm{SMP}}(T_{\mathrm{S}}(t)) + [C_P^{\mathrm{AD,S}}(T_{\mathrm{S}}(t)) \\ &\quad - C_P^{\mathrm{AD,R}}(T_{\mathrm{R}}(t))] - [C_P^{\mathrm{AD,S}}(T_{\mathrm{S0}}(t)) \\ &\quad - C_P^{\mathrm{AD,R}}(T_{\mathrm{R}}(t))] \\ &= C_P^{\mathrm{SMP}}(T_{\mathrm{S}}(t)) + [C_P^{\mathrm{AD,S}}(T_{\mathrm{S}}(t)) \\ &\quad - C_P^{\mathrm{AD,S}}(T_{\mathrm{S0}}(t))] \end{aligned} \tag{22}$$

The corrected value $C_P^{X\mathrm{Corr1}}$ is closer to the desired C_P^{SMP}, because the assumption in Eq. (4) is not required any more.

For the experiment illustrated in Figs. 3, 6 and 7, the difference in addenda of the reference and sample sensors is about 1% of the addenda. This minuscule mismatch is the result of careful selection of two sensors, which typically should be in adjacent positions on the wafer. For a pair of sensors from the same wafer, but from opposite sections of it, the difference in addenda can achieve 10%. The mismatch can be even more for sensors from different wafers.

3.3.2. Correction for different heat capacity of blank sample cell at different temperatures

The assumption in Eq. (5) is equivalent to the supposition that the heat capacity of an empty cell does not depend on temperature, which is generally not true. At any given time t, the temperature of the sample cell in an experiment where a sample is present is different (typically, lower) from the corresponding idle experiment. These two facts make the difference $C_P^{\mathrm{AD,S}}(T_{\mathrm{S}}(t)) - C_P^{\mathrm{AD,S}}(T_{\mathrm{S0}}(t))$ in Eq. (22) non-zero. Straightforward calculation of $C_P^{\mathrm{AD,S}}(T)$ can be made from the idle experiment using Eq. (2b) without the C_P^{SMP} term. Then, for each time t, the value of the second correction can be found:

$$C_P^{X2}(t) = C_P^{\mathrm{AD,S}}(T_{\mathrm{S}}(t)) - C_P^{\mathrm{AD,S}}(T_{\mathrm{S0}}(t)). \tag{23}$$

Subtracting this term from value $C_P^{X\mathrm{Corr1}}$ (see Eq. (22)), the sample heat capacity can be found

$$\begin{aligned} C_P^{X\mathrm{Corr12}}(t) &= C_P^{X}(T_{\mathrm{S}}(t)) - C_P^{X1}(T_{\mathrm{S0}}(t)) - C_P^{X2}(t) \\ &= C_P^{\mathrm{SMP}}(T_{\mathrm{S}}(t)) \end{aligned} \tag{24}$$

It should be noted, that the $C_P^{\mathrm{AD,S}}(T)$ calculated by Eq. (2a) is extremely noisy and, used "as is", will ruin the result. Assuming that the heat capacity of an empty cell, which consists only of silicon nitride and metal, has no features in a given temperature range and is inherently very smooth, the

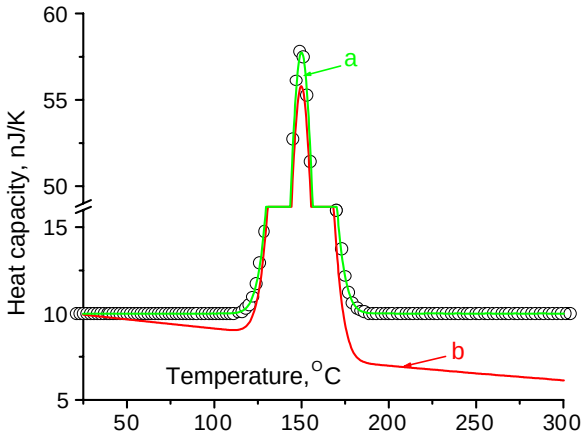

Fig. 5. Calorimetric curves calculated with and without the second correction. Calculations are made by the main method and use computer simulated raw data. (○)—imitated sample $C_P(T)$ dependence, the same as in Fig. 4. (a) first and second corrections are made, (b) only first correction is made. In the raw data generation, two sensors are simulated; these sensors have different $T(R)$ characteristics and equal addenda heat capacities, which linearly depend on temperature.

$C_P^{\mathrm{AD,S}}(T)$ can be approximated by a smooth analytical function. Typically, we use fourth-order polynomial approximation. Transient processes generated by switching current on and off at the beginning and at the end of a scan generally cause noticeable deviation of the first and the last points of experimental $C_P^{\mathrm{AD,S}}(T)$ plot. Deviated points, which are far from the average noise level of a smooth monotonic function should be removed prior to the approximation. Typical result of this correction is shown in Fig. 5. This correction is especially important for temperatures above where strong thermal effects in the sample (melting, sublimation etc.) occur, when the difference in the temperature of the sample sensor with and without sample has increased.

3.3.3. Correction for heat loss

For all previous considerations we assume adiabatic conditions of calorimetric experiments. This is true, strictly speaking, only for an infinitely high heating rate. In real experiments, the calculated heat capacity of cells includes heat loss during the scan. For the sample cell in an idle experiment we can write:

$$P_{\mathrm{HEAT}}(t) + P_{\mathrm{HL}}(t) = v_{\mathrm{S0}}(t) C_P^{\mathrm{AD,S}}(t), \tag{25}$$

where P_{HEAT} is the part of electric power consumed by the heating of the calorimetric cell and P_{HL} is the power of heat loss. $C_P^{\mathrm{AD,S}}$ here means effective heat capacity of the cell. Introducing $C_P^{\mathrm{AD0,S}} = P_{\mathrm{HEAT}}/v_{S0}$ as the real heat capacity of the sample cell (when heat loss is negligible), which depends only on temperature, we can rewrite Eq. (25) as

$$C_P^{\mathrm{AD,S}}(t) = C_P^{\mathrm{AD0,S}}(T_{\mathrm{S0}}(t)) + \frac{P_{\mathrm{HL}}(t)}{v_{\mathrm{S0}}(t)}, \tag{26}$$

Generally, heat loss at a given time t depends on the whole prehistory of the heating. However, for the first approximation we can assume that heat loss depends on the current temperature of the cell only—$P_{\mathrm{HL}}(t) = P_{\mathrm{HL}}(T(t))$. This assumption gives us the opportunity to rewrite Eq. (26) as:

$$C_P^{\mathrm{AD,S}}(T_{\mathrm{S0}}) = C_P^{\mathrm{AD0,S}}(T_{\mathrm{S0}}) + \frac{P_{\mathrm{HL}}(T_{\mathrm{S0}})}{v_{\mathrm{S0}}(T_{\mathrm{S0}})}. \tag{27}$$

This means that running the idle experiment at different heating rates v_{S_0}, we can calculate P_{HL} for the whole temperature range of the experiment. Practically, heat capacities for an empty sample cell at several different heating rates $C_P^{\mathrm{AD,S}}(T_{\mathrm{S0}}, v_{\mathrm{S0}})$ are calculated and then approximated by smooth analytical functions as described in section 3.3.2. The heating rates v_{S_0} should also be approximated by smooth analytical functions; for this parameter, we also typically use fourth-order polynomial approximation. Then, for each given T_{S0}, parameters $C_P^{\mathrm{AD0,S}}$ and P_{HL} can be found by a linear fit of the dependence $C_P^{\mathrm{AD,S}}(1/v_{\mathrm{S0}})$. Typical heat loss dependence versus temperature during a calorimetric scan is shown in Fig. 6.

In order to use $P_{\mathrm{HL}}(T_{\mathrm{S0}})$ for heat capacity correction, it should be noted that heat loss in the idle experiment and the experiment with the sample is different due to a decrease in the heating rate after sample loading. Using the cell's heat capacity as a function of both temperature and heating rate, we can correct Eq. (24), omitting time dependence for clarity

$$\begin{aligned} C_P^{X\mathrm{Corr12}} &= C_P^X - C_P^{X1} - C_P^{X2} \\ &= [C_P^{\mathrm{SMP}}(T_{\mathrm{S}}) + C_P^{\mathrm{AD,S}}(T_{\mathrm{S}}, v_{\mathrm{S}}) - C_P^{\mathrm{AD,R}}(T_{\mathrm{R}}, v_{\mathrm{R}})] \\ &\quad -[C_P^{\mathrm{AD,S}}(T_{\mathrm{S0}}, v_{\mathrm{S0}}) - C_P^{\mathrm{AD,R}}(T_{\mathrm{R}}, v_{\mathrm{R}})] \\ &\quad -[C_P^{\mathrm{AD,S}}(T_{\mathrm{S}}, v_{\mathrm{S0}}) - C_P^{\mathrm{AD,S}}(T_{\mathrm{S0}}, v_{\mathrm{S0}})] \\ &= C_P^{\mathrm{SMP}}(T_{\mathrm{S}}) + [C_P^{\mathrm{AD,S}}(T_{\mathrm{S}}, v_{\mathrm{S}}) - C_P^{\mathrm{AD,S}}(T_{\mathrm{S}}, v_{\mathrm{S0}})] \end{aligned} \tag{28}$$

The difference $[C_P^{\mathrm{AD,S}}(T_{\mathrm{S}}, v_{\mathrm{S}}) - C_P^{\mathrm{AD,S}}(T_{\mathrm{S}}, v_{\mathrm{S0}})]$ in Eq. (28) can be expressed using Eq. (27), and the correction for heat loss C_P^{X3} can be found:

$$\begin{aligned} C_P^{X3}(t) &= C_P^{\mathrm{AD,S}}(T_{\mathrm{S}}(t), v_{\mathrm{S}}(t)) - C_P^{\mathrm{AD,S}}(T_{\mathrm{S}}(t), v_{\mathrm{S0}}(t)) \\ &= \frac{P_{\mathrm{HL}}(T_{\mathrm{S}})}{v_{\mathrm{S}}(t)} - \frac{P_{\mathrm{HL}}(T_{\mathrm{S}})}{v_{\mathrm{S0}}(t)}. \end{aligned} \tag{29}$$

Fig. 7 illustrates the effect of C_P^{X3} correction. The correction is especially important for samples that undergo strong endothermic processes in a narrow temperature range (e.g. melting). During such a process the sample temperature changes slowly, and heat loss, which is roughly proportional to time, increases significantly.

An additional correction can be made if we note that the presence of sample in the cell changes heat loss at a given time t not only because it causes a decrease in temperature and heating rate, but also because it provides an additional method of heat loss—heat conductivity through the sample; the emissivity can also be changed. Assuming this,

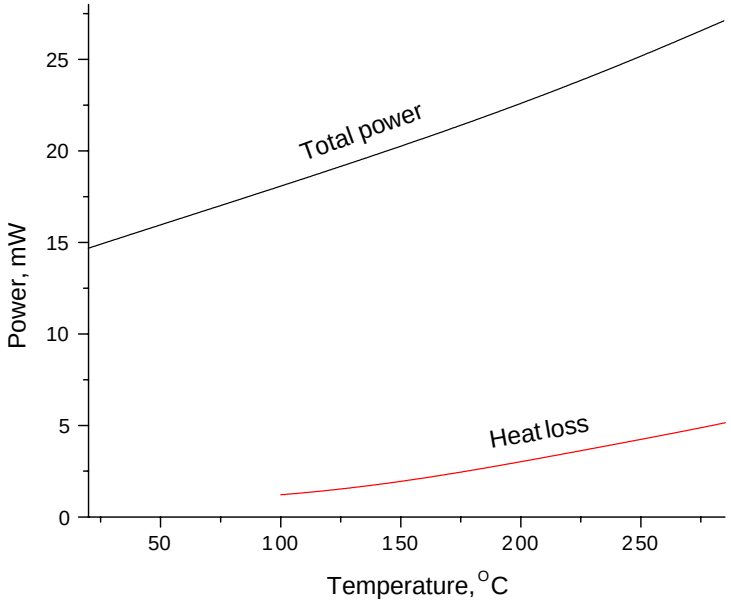

Fig. 6. Heat loss for a typical sample sensor without sample on it. This sensor was used for measurements illustrated on Figs. 3 and 7. Total power input for 35 K/ms average heating rate is shown for comparison.

the numerator in the first term of the expression for C_P^{X3} (Eq. (29))—P_{HL}—should be replaced by the heat loss power for the cell with sample $P_{\mathrm{HL}}^{+\mathrm{S}}$. This replacement is equivalent to introducing an additional correction C_P^{X4}:

$$C_P^{X4}(t) = \frac{P_{\mathrm{HL}}^{+\mathrm{S}}(T_{\mathrm{S}})}{v_{\mathrm{S}}(t)} - \frac{P_{\mathrm{HL}}(T_{\mathrm{S}})}{v_{\mathrm{S}}(t)}. \tag{30}$$

Parameter $P_{\mathrm{HL}}^{+\mathrm{S}}$ can be found using the same procedure, as used for P_{HL} calculation, but using data from the experiment with sample. Unlike P_{HL} calculation, where $C_P^{\mathrm{AD,S}}(T)$ (and, consequently, $v_{\mathrm{S}_0}(T)$) curves are inherently smooth and highly monotonic and can be effectively approximated by simple analytical functions, $[C_P^{\mathrm{AD,S}} + C_P^{\mathrm{SMP}}](T)$ and $v_{\mathrm{S}}(T)$ curves may have significant features (in case of pronounced phase transitions in a massive sample) and effective smoothing/approximation of such data can be a challenge. Additional care should be taken in using of C_P^{X4} correction if the heat effects in the sample depend on heating rate, for example, in the temperature range of a glass transition or other kinetically driven process.

Finally, the sample heat capacity, corrected by all four corrections can be written:

$$C_P^{X\mathrm{Corr1234}}(t) = C_P^{X}(t) - \sum_{k=1}^{4} C_P^{Xk}(t) = C_P^{\mathrm{SMP}}(T_{\mathrm{S}}(t)). \tag{31}$$

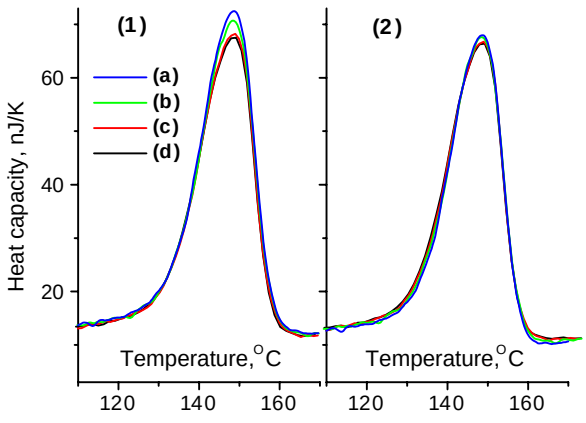

Fig. 7. Calorimetric curves calculated with and without the third correction. Calculations are made by the main method and use experimental data for 2 nm thick In film deposited on sensor with Ni metallization. Curves correspond to different heating rates: (a) 35 K/ms, (b) 50 K/ms, (c) 110 K/ms, (d) 150 K/ms. Plots: (1) 1,2 corrections are made, (2) 1–3 corrections are made.

Fig. 8 shows the effect of C_P^{X4} correction. This is especially important when the sample has significant heat conductivity (a thick film, for example) and covers the entire sensor, which allows heat to flow from the cell through the sample to the silicon frame.

3.3.4. Common notes about corrections

Not all corrections have the same importance. The first correction C_P^{X1} is used practically in all cases, and both for main and simplified methods of calculations. The second C_P^{X2} and third C_P^{X3} corrections are usually used when improved accuracy is required and the main calculation method is used. The forth correction C_P^{X4} is used more rarely.

Even using of all mentioned corrections does not guarantee ultimate accuracy. Additional investigations are required, particularly for more accurate heat loss evaluation, which can be made by detailed numerical calculation of heat balance of the sensor during the calorimetric scan.

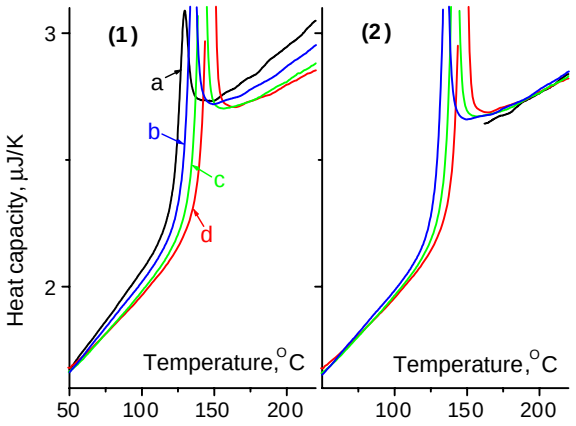

Fig. 8. Calorimetric curves calculated with and without the fourth correction. Calculations are made by the main method and use experimental data for 400 nm thick poly(2-vinyl pyridine) film spin cast on a sensor with a thick SiN_x membrane (400 nm) and Pt metallization. Curves correspond to different heating rates: (a) 15–25 K/ms, (b) 30–45 K/ms, (c) 60–90 K/ms, (d) 100–140 K/ms. Plots: (1) 1–3 corrections are made, (2) 1–4 corrections are made.

A typical experimental schedule, which allows us to use the main method of calculation with corrections, is as follows. Prior to the experiment, both the sample and reference sensors are calibrated. Then an idle experiment is performed with different heating rates. Three to four different rates can be used for systems where no dependence of heating rate is expected, and six to eight otherwise. Next, experiments with sample are made using the same heating rates for the reference sensor, as in the idle experiment.

3.4. Temperature versus resistance calibration

As was mentioned in Section 2, the resistance of heater R is calibrated against temperature T prior to a calorimetric experiment. This measurement is performed in a vacuum three-zone tube furnace. R is measured by four point probe method, and corresponding T is measured using a standard platinum RTD (100 Ω, class A, tolerance less than 1 K in the range from −200 to +500 °C). Details of the calibration procedure are described elsewhere [8]. Both sample and reference sensors should be calibrated for accurate measurements.

3.4.1. Correction of the heating during resistance measurement

The four-point probe method of resistance measurement applies a current I_{CAL} through a resistor. This current causes heating of the resistor to the temperature $T_{AMB} + \Delta T$, where T_{AMB} is ambient temperature and ΔT is additional heating caused by I_{CAL}. In order to determine the resistance at exactly T_{AMB}, let us assume that ΔT is proportional to the power of Joule heat $P = I_{CAL}^2 R$, and R depends linearly on the T (in the small temperature range ΔT). Making two measurement with different currents, I_{CAL1} and I_{CAL2} (where $I_{CAL1} < I_{CAL2}$), and denoting measured resistances as R_{CAL1} and R_{CAL2}, respectively, we can find:

$$\begin{aligned} R(T_{AMB}) &= R|_{P=0} \\ &= R_{CAL1} - \frac{R_{CAL2} - R_{CAL1}}{(I_{CAL2}^2 R_{CAL2}/I_{CAL1}^2 R_{CAL1}) - 1} \\ &\approx R_{CAL1} - \frac{R_{CAL2} - R_{CAL1}}{(I_{CAL2}/I_{CAL1})^2 - 1} \end{aligned} \quad (32)$$

Typically, for measuring resistance in the calibration procedure, we use a Hewlett–Packard 34420A nanovolt/microohmmeter. For on-sensor heater resistance, $I_{CAL1} = 100\,\mu A$ and $I_{CAL2} = 1\,mA$ are used. For smaller currents (10 μA, for example) the heating effect is negligible, but the deterioration of measurement accuracy at such small currents makes them impractical. Measurement of the standard RTD resistance is made with $I_{CAL} = 1\,mA$ and no noticeable heating is detected.

3.4.2. Correction of the shunting effect

At elevated temperatures, the insulation properties of the SiN_x layer between the sensor metallization and the silicon frame degrade (Fig. 9f). In this case, the current through the insulation and silicon shunts the sensor heater and the measured resistance (Fig. 9a) becomes smaller than the actual. This effect is observed only in the calibration and not in the calorimetric measurements. During the DSC scan, the silicon frame of the sensor remains cold and provides no significant conductivity.

While a complete solution to this problem would require a redesign of the sensor [8], the use of a simple model can significantly improve experimental $R(T)$ dependence. This model represents the sensor as a network of resistors, shown in Fig. 10. It is assumed that all R_{SiN} resistances are the same

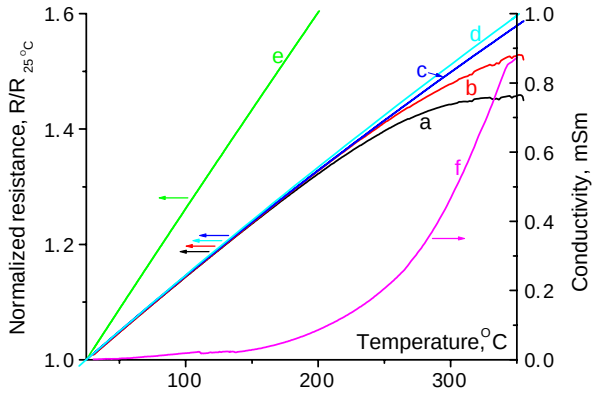

Fig. 9. Resistive properties of sensors as functions of temperature. All curves are shown for sensors with platinum metallization; resistances are shown in the normalized form. (a) typical experimental dependence for sensor with regular (~50 nm thick) SiN_x membrane, after correction by Eq. (32). (b) the same dependence corrected for shunting effect by Eq. (34). (c) the same data after approximation by method IV. (d) typical experimental dependence for sensor with thick (~400 nm) SiN_x membrane, where shunting effect is negligible in this temperature range (after correction by Eq. (32)). (e) dependence for bulk platinum. (f) conductivity between metallization and back side of sensor with regular membrane.

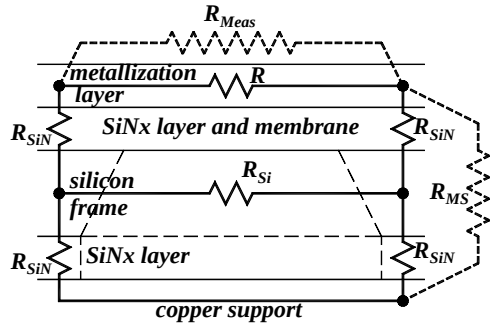

Fig. 10. Model of the shunting effect. Thick dashed lines denote modeled "resistors". Thin lines denote the different layers of material in the sensor.

and much larger than both the resistance of the metallization R_{MET} (which is about the same as the resistance of the heater R) and the resistance of the silicon frame R_{Si}. In order to use this model, the support for the sensor should be conductive and the resistance between metallization and the support R_{MS} should be measured during the calibration procedure also. Obviously:

$$\begin{cases} R_{\mathrm{MS}} = R_{\mathrm{SiN}} \\ \dfrac{1}{R_{\mathrm{Meas}}} = \dfrac{1}{R} + \dfrac{1}{2R_{\mathrm{SiN}}} \end{cases}, \tag{33}$$

where R_{Meas} is the measured heater resistance. Consequently:

$$R = \frac{1}{(1/R_{\mathrm{Meas}}) - (1/2R_{\mathrm{MS}})}. \tag{34}$$

3.4.3. Approximation of the calibration curve by analytical function

A properly chosen approximation method can improve the correction for shunting effect. It is reasonable to assume that the $R(T)$ dependence for a heater made using metal Me will resemble the bulk behavior $R_{\mathrm{BULK}}(T)$ (method IV). In practice, the $R(R_{\mathrm{BULK}})$ function (where R and R_{BULK} are at the same temperature) can be approximated well by a second order polynomial:

$$R_{\mathrm{APP}} = \sum_{i=0}^{2} a_i R_{\mathrm{BULK}}^i. \tag{35}$$

The a_2 coefficient can be used as a good estimation of sensor quality (regarding the shunting effect). It should be noted that, even for model systems without shunting (for example, metallization on an SiO_2 substrate) $a_2 \neq 0$, although it is very small. Approximation with Eq. (35) is effective if the least square method (LSM) is used with the errors of R as weighting coefficients. Typically, good estimation for error in R is given by:

$$\Delta R(T) = \sqrt{(R(T) - R_{\mathrm{Meas}}(T))^2 + \left[\alpha \left(\frac{\mathrm{d}R}{\mathrm{d}T}\right)_{\mathrm{AVR}}\right]^2}, \tag{36}$$

where $\alpha = 1\,\mathrm{K}$ (accuracy of the temperature measurements in the calibration system) and $(\mathrm{d}R/\mathrm{d}T)_{\mathrm{AVR}}$ is an estimation

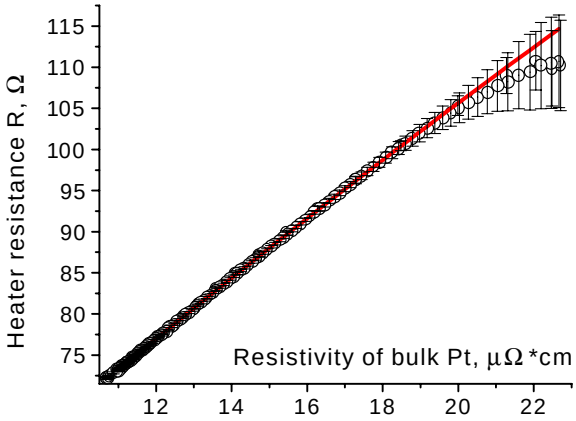

Fig. 11. Heater resistance approximation. (○) – data points, corrected by Eqs. (32) and (34), error bars are calculated using Eq. (36). Thick line represents second-order polynomial approximation.

of the slope of $R(T)$. An example of this approximation is given in Fig. 11. Improvement of the $R(T)$ dependence is illustrated in Fig. 9 (compare curves (b)—before and (c)—after approximation, and (d)—typical dependence for special sensors without shunting effect at moderate temperatures).

The final operation is the approximation of the $T(R)$ function, which is used in C_P calculation, by fourth-order polynomial:

$$T_{\mathrm{APP}} = \sum_{i=0}^{4} b_i R_{\mathrm{APP}}^i.$$

4. Heat capacity analysis discussion

The methods of heat capacity analysis described above, have been used to study various material systems using the nanocalorimetry technique. These material systems include ultra-thin (down to 1–3 nm thick) polymer films [17–19], isolated microscopic crystals of polymers [20], discontinuous indium deposits of sub-nanometer average thickness [9,21], and self-assembled monolayers. Interesting effects are found. For example: discrete periodic melting peaks are observed in the heat capacity data of 2–4 nm indium clusters, which are presumably caused by preferable formation of clusters with complete shell of atoms at particle surface [21]; a pronounced glass transition is observed in thin spin-cast films of polystyrene, poly (methyl methacrylate) and poly (2-vinyl pyridine) on platinum substrates even at thickness as small as 1–3 nm, and no appreciable dependence of the glass transition temperature is detected over the thickness range from hundreds of nanometers down to 3 nm thick films [17]. We hope this paper on one of the key aspects of the TDSC technique—the method of data analysis—will encourage the implementation of this promising technique by other research groups.

While the described calculation methods are successful so far, they are far from ideal and there are issues to be

addressed in the future development. One of the important problems is taking the heat loss into account in a more accurate way than the described linear approach. The methods presented require several parameters (smoothing, etc.) which are chosen on the basis of the experimentalist's intuition and experience. Optimization of these parameters is another serious problem. While sensors can withstand elevated temperatures (>600 °C), the calibration procedure, described here, typically can not provide reliable calibration curves for temperatures above 350–400 °C. Development of calibration procedure, suitable for elevated temperatures, will be important contribution for high-temperature applications of TDSC method.

5. Conclusions

The thin-film differential scanning calorimetry (TDSC) or nanocalorimetry is a powerful tool for investigation of thermal properties of nanometer- thick films in a wide temperature range. The quality of results obtained by this method strongly depends on the data processing algorithms. The formulas, algorithms and models, discussed above, have been effective analysis tool in addressing the following issues:

- attenuation of the noise component caused by differentiation procedure of raw data;
- reduction of the deviations in calorimetric curves, caused both by initial mismatch of sample and reference sensors, and by the addition of sample on the sensor;
- decrease of the spurious effect of heat loss during the calorimetric scan;
- compensation of the errors in the calibration procedure caused both by heating of the sensor by probing current and by significant shunting effect at elevated temperatures.

Acknowledgements

This work was supported through National Science Foundation DMR 0108694.

References

[1] A.G. Worthing, Phys. Rev. 12 (1918) 199.
[2] N.S. Rasor, J.D. McClelland, Rev. Sci. Instrum. 31 (1960) 595.
[3] M.S. Wire, Z. Fisk, G.W. Webb, Rev. Sci. Instrum. 56 (1985) 1223.
[4] B. Fröchte, Y. Khan, E. Kneller, Rev. Sci. Instrum. 61 (1990) 1954.
[5] O.F. Shlensky, L.N. Aksenov, A.G. Shashkov, Thermal Decomposition of Materials, Elsevier, Amsterdam, The Netherlands, 1991.
[6] E.D. Nikitin, P.A. Pavlov, P.V. Skripov, J. Chem. Thermodyn. 25 (1993) 869.
[7] D.W. Denlinger, E.N. Abarra, K. Allen, P.W. Rooney, M.T. Messer, S.K. Watson, F. Hellman, Rev. Sci. Instrum. 65 (1994) 946.
[8] E.A. Olson, M.Yu. Efremov, M. Zhang, Z.S. Zhang, L.H. Allen, J. MEMS 12 (2003) 355.
[9] M. Zhang, M.Yu. Efremov, F. Schiettekatte, E.A. Olson, A.T. Kwan, S.L. Lai, T. Wisleder, J.E. Greene, L.H. Allen, Phys. Rev. B 62 (2000) 10548.
[10] S.L. Lai, G. Ramanath, L.H. Allen, P. Infante, Z. Ma, Appl. Phys. Lett. 67 (1995) 1229.
[11] S.L. Lai, G. Ramanath, L.H. Allen, P. Infante, Appl. Phys. Lett. 70 (1997) 43.
[12] M. Yu. Efremov, E.A. Olson, M. Zhang, Z.S. Zhang, L.H. Allen, submitted to Rev. Sci. Instrum.
[13] D.R. Hartree, Numerical Analysis, Oxford University Press, London, 1952, pp. 116–118.
[14] B. Carnahan, H.A. Luther, J.O. Wilkes, Applied Numerical Methods, Wiley, NY, 1969, p. 128.
[15] W.J. Karplus, W.W. Soroka, Analog Methods, second ed., McGraw-Hill, New York, 1959, pp. 28–31.
[16] T.D. Truitt, A.E. Rogers, Basics of Analog Computers, John F. Rider Publisher Inc., New York, 1960, pp. 1-96–1-103.
[17] M.Yu. Efremov, E.A. Olson, M. Zhang, Z.S. Zhang, L.H. Allen, Phys. Rev. Lett. 91 (2003) 085703.
[18] M.Yu. Efremov, J.T. Warren, E.A. Olson, M. Zhang, A.T. Kwan, L.H. Allen, Macromolecules 35 (2002) 1481.
[19] M.Yu. Efremov, E.A. Olson, M. Zhang, L.H. Allen, Thermochim. Acta 403 (2003) 37.
[20] A.T. Kwan, M.Yu. Efremov, E.A. Olson, F. Schiettekatte, M. Zhang, P.H. Geil, L.H. Allen, J. Polym. Sci., Part B: Polym. Phys. 39 (2001) 1237.
[21] M.Yu. Efremov, F. Schiettekatte, M. Zhang, E.A. Olson, A.T. Kwan, R.S. Berry, L.H. Allen, Phys. Rev. Lett. 85 (2000) 3560.